Volume 18, Number 3, 2025. pp. 411-422

Jordan Journal of Physics

ARTICLE

Synergistic Antibacterial Properties of Zinc Oxide Nanoparticles Embedded in Chitosan and PVA Composite

Saif M. Alghazaly, Khalid H. Hatif Al-Atiya and **Hikmat A. J. Banimuslem**

Department of Physics, College of Science, University of Babylon, Babel, Iraq.

Doi: **https://doi.org/10.47011/18.3.13**

Received on: 22/07/2024; *Accepted on: 09/10/2024*

Abstract: In this study, zinc oxide nanostructures were synthesized via the sol-gel technique and characterized utilizing XRD, FE–SEM, FT–IR, and UV–vis. The solution casting approach was used to insert zinc oxide nanoparticles (ZnO NPs) into a series of chitosan and polyvinyl alcohol (Cs/PVA) mix films. X-ray diffraction (XRD) analysis demonstrated that increasing the ZnO nanostructures wt% leads to structural changes in the Cs/PVA blend. UV–vis analysis showed that with increased zinc oxide nanoparticles, the optical bandgap of Cs/PVA decreased from 5.45 to 4.5 eV. The antimicrobial tests revealed that the nanocomposite films demonstrated significantly improved antimicrobial effectiveness compared to the pure Cs/PVA film. This improvement directly corresponds to the increasing concentration of ZnO nanoparticles within the matrix. This nanocomposite can be used as a filter against *Brevibacterium epidermidis,* a bacterium responsible for unpleasant odor during sweating and when wearing shoes for long periods.

Keywords: Cs/PVA, Zinc oxide nanoparticles, Sol-gel, Optical bandgap, *Brevibacterium epidermidis*.

Introduction

Zinc oxide (ZnO) is an inorganic compound found naturally in the earth's crust, though most commercially used zinc oxide is synthetically produced [1]. It has the chemical formula ZnOand often appears as a white powder that is essentially insoluble in water. ZnO is one of the most studied materials and is employed in many electronic, healthcare, and environmental applications, confirming its significance to modern life. Because of this, ZnO is crucial in many industries and allows for fresh answers to modern challenges. Its characteristics encompass a high electrochemical coupling coefficient, exceptional photostability, wide radiation absorption, and remarkable chemical stability [2]. ZnO powder is widely applied across industries, including in paints, catalysts, and various technological, medical, and industrial applications, where particle size plays a crucial role. Therefore, many synthetic methods have been developed for the substance, such as sol-gel, precipitation, green leaf extract, microwave, wet chemical, and hydrothermal methods, which have succeeded in nanoparticle formation [3]. Among all the nanoparticle synthesis methods, sol-gel has attracted a lot of attention as an efficient, easy-to-process, and low-cost technique [4]. The sol-gel (SG) process typically unfolds in four stages: dissolution, hydrolysis, polymerization, and conversion to isolated ZnO solid powder [5]. Given the natural antimicrobial activity of chitosan, a biopolymer, it can be helpful in synthesizing antibacterial hydrogels. Most of the chitosan-based hydrogels have proven to exhibit good antibacterial effects on several microbial forms, such as bacteria, yeast, mold, and algae [6]. Chitosan (Cs) is an intriguing natural biopolymer with multiple

Corresponding Author: Saif M. Alghazaly **Email**: sci.saif.mohamed@uobabylon.edu.iq

desirable characteristics, namely, biocompatibility, biodegradability, non-toxicity, odorlessness, and the solubility of the chemical modifications. This is important because of the challenges associated with the disposal of synthetic polymers that result in environmental pollution [7]. Chitosan can be modified by blending with other materials, altering its chemical properties, or incorporating it with other polymers and inorganic particles. Through physical blending and cross-linking, the functionality of chitosan-based materials can be enhanced, thereby extending their applications. Additionally, chemical treatments can further improve the solubility and mechanical properties of chitosan [8, 9]. A blend of chitosan and polyvinyl alcohol (PVA) is particularly attractive due to its favorable mechanical, physical, and chemical characteristics. A number of features explain why PVA is selected: good mechanical properties, biodegradability, ease of preparation, high film-forming ability, and excellent chemical resistance [10]. Incorporation of such materials has attracted growing interest for antibacterial and antifungal applications. Wearing closed shoes, sweating, and having sensitive feet are some of the causes of foot odor. Closed shoes create a confined and humid environment that restricts air circulation, retains moisture, and promotes bacterial growth, which in turn leads to unpleasant odors [11]. Hyperhidrosis, characterized by excessive sweating, creates an optimal habitat for the proliferation of bacteria and fungi, contributing to odor in dark, warm, and moist areas of the body [12]. Two newly identified species of the genus *Brevibacterium* have been found in dairy and skin samples. The strains obtained from cheese and milk, specifically identified as *Brevibacterium casei*, are the culprits behind the distinctive aroma of cheese. *Brevibacterium epidermidis,* commonly found on human skin, is responsible for body odor. The skin debris shed by humans serves as a food source for the *Brevibacterium* bacteria. Because most people wear shoes and socks when walking, they provide an ideal environment for these microbes, as they thrive in warm, damp environments. *Brevibacterium* converts the amino acid methionine into the volatile molecule methanethiol (CH_3SH), which has a strong and disagreeable odor [13, 14]. This research aims to manufacture zinc oxide nanoparticles and study their structural properties, as well as the effect of incorporating them into Cs/PVA blend films. The resulting nanocomposites hold potential for use in deodorant formulations and as protective shoe linings, serving as promising candidates against *Brevibacterium epidermidis*, the bacterium responsible for unpleasant odors associated with sweating and prolonged shoe use.

Experimental Part

Materials

Chitosan $(C_6H_{11}NO_4)n$, medium molecular weight (300-1000 cps, average M.W.=1250000) was obtained from Glentham Life Sciences Ltd, United Kingdom. Polyvinyl alcohol (PVA) $(C_2H_4O)n$ was obtained from Central Drug House (P) Ltd., India [M.W. = 85000 to 124000]. Zinc acetate (ZA) $(CH_3COO)_2Zn$ $2H_2O$, [M.W. = 219.49] and acetic acid (CH3COOH) 99.5% [M.W. = 60.05] were obtained from Thomas Baker, India. Sodium hydroxide (NaOH) [M.W. = 40] was supplied by SDFCL, India. All chemicals and reagents used in this study were of analytical grade and were employed without further purification.

Preparation of ZnO Nanoparticles (ZnO NPs)

ZnO nanoparticles were synthesized using zinc acetate as the precursor, ethanol as the solvent, and sodium hydroxide as the catalyst, following a sol-gel-based procedure [15,16]. Specifically, 5.402 g of zinc acetate was dissolved in 200 mL of ethanol and stirred vigorously at room temperature with a magnetic stirrer. The solution was sonicated for 15 minutes until it became clear. Subsequently, the pH was adjusted to 8 by the dropwise addition of 40 mL of 1 M NaOH. The reaction mixture was stirred for 3 hours to ensure completion, then left undisturbed for 24 hours to allow for precipitation. The resulting product was dried at 70 °C in an electric oven, followed by calcination at 400 °C for 3 hours to remove residual impurities and obtain highly crystalline ZnO nanoparticles.

Nanocomposites (ZnO/CS-PVA) Sample Preparation

Nanocomposite films were prepared using the solution casting method. First, 5 g of chitosan was dissolved in 480 mL of a 2% (v/v) aqueous acetic acid solution and stirred vigorously at 50 °C for 2 h until a clear solution was obtained. Next, 5 grams of PVA were dissolved in 200 mL

of deionized water and stirred vigorously with a magnetic stirrer at 50 °C for 1 hour until a homogeneous solution was achieved. The slow addition of the PVA and CS solutions ensures proper mixing. Prolonged stirring helps in the dispersion of any large particles or lumps, yielding a more homogeneous product. Upon mixing, the polymer chains of PVA and CS were able to interact through hydrogen bonding between hydroxyl OH^- and amino (NH^{2-}) groups, stabilizing the blended solution and promoting the formation of a coherent material. It should also be noted that some experimentation may require the sample to be stirred for different durations depending on the volume of the solutions used, as well as the concentrations of PVA and CS used in the experiment. The first model of the pure membrane containing no nanoparticles was cast into a 10 cm diameter plastic dish. A series of ZnO/CS-PVA membranes with different nanohybrid content was prepared by adding appropriate amounts of ZnO nanoparticles to the CS/PVA solution. The nanohybrid content levels mentioned were 2.5, 5, 7.5, 10, 12.5, and 15 wt/wt percent. The accurate quantity of ZnO nanoparticles was dispersed in 10 mL of distilled water. The ZnO nanoparticle suspension was then agitated to make sure that the nanoparticles were well dispersed. The suspension was then put in an ultrasound machine for 15 minutes in order to increase the nanoparticles' dispersion and to eliminate the agglomeration. The well-dispersed ZnO nanoparticle suspension was later added to the CS-PVA solution that was prepared earlier. Stirring was carried out for 20 minutes to guarantee the homogenization of the Cs-PVA/ ZnO nanoparticles throughout the solution, including the distribution of ZnO nanoparticles in the Cs-PVA matrix. The ZnO/CS-PVA solution samples were then cast into plastic dishes or molds. The cast samples were transferred to an oven at a temperature of 45 °C to dry the films for three days.

Characterization Methods

Structural investigations of the synthesized ZnO nanoparticles and ZnO/CS-PVA hybrid films were conducted using XRD (600 Miniflex, Rigaku, Japan) with a Bruker D8 advanced powder XRD, utilizing a CuKα radiation source (λ = 1.5417 Å, I = 0.05 A, V = 40 keV). The scan rate was set at 3° per minute, covering a 2θ range from 40° to 70°. The Fourier transform approach was employed to analyze infrared spectra of very intricate combinations using an FTIR analysis instrument, IR Affinity-1, made in Kyoto, Japan. The surface morphology of ZnO nanoparticles and nanocomposites was analyzed using a field-emission scanning electron microscope (FE-SEM) (Ltd., Tokyo, Japan) equipped with an X-Act EDS detector from Oxford Instruments, Abingdon, United Kingdom. Optical characterization was conducted at room temperature using a SHIMADZU UV-1800 spectrophotometer, covering the ultraviolet and visible light (UV-vis) wavelength range from 200 to 800 nm.

Brevibacterium Epidermidis Bacteria Activity Assay

Brevibacterium epidermidis is an obligate aerobe, mesophilic, Gram-positive bacterium commonly isolated from human skin and classified under the genus *Brevibacterium* [17]. It is rod-shaped and includes species of both biotechnological and clinical relevance. Although *Brevibacterium epidermidis* is not typically associated with pathogenesis, it has been implicated in infections such as bacteremia in immunocompromised patients with central venous catheters [18]. It is an irregular Gram-positive rod resembling corynebacteria and is also found in dairy products, where it contributes to aroma and coloration [18].

Understanding its characteristics, antimicrobial susceptibility, and clinical implications is important for evaluating potential therapeutic and preventive strategies. The magnitude of the inhibition zone is directly proportional to the antibacterial activity of the tested material, reflecting its inhibitory effect on bacterial growth [19].

The antibacterial activity of the nanocomposites was evaluated using the agar disk diffusion method, a simple and cost-effective technique widely applied for antimicrobial testing. Sterile Mueller-Hinton agar (20 mL) was poured into 10 cm diameter Petri dishes. After the media solidified, 0.1 mL of bacterial suspension was evenly spread on the surface. Following a 5-minute absorption period, 6 mm diameter disks of each nanocomposite (NC) sample were placed in the center of the plates. The pure polymer mixture served as the control. The dishes were incubated at 37 °C for 24 hours [20, 21]. The inhibition zones were measured in millimeters, and each test was

performed in triplicate for all prepared nanomembrane models.

Results and Discussion

Fourier-transform Infrared Spectroscopy (FT-IR)

Figure 1 presents the FT-IR spectrum used to analyze and identify the functional groups of ZnO nanoparticles produced via the sol-gel method. As reported previously in the literature [22], the FT-IR spectrum revealed a broad absorption band at 408 cm^{-1}, attributed to the Zn-O stretching vibration. To verify these findings, previous literature was consulted, confirming that all peaks appeared around 400 cm^{-1}. Additionally, peaks were identified at 2939 and 2854 cm^{-1}, attributed to the CH_3 group's symmetric and asymmetric stretching frequencies [23]. A peak at 1651 cm^{-1} is characteristic of the hydroxyl group (O-H). However, the peaks at 1047 1/cm may be ascribed to the stretching modes of carbon-oxygen bonds and indicate lattice vibration of the absorption peaks. These findings are similarly reported elsewhere [24]. Moreover, stretching of the hydroxyl group can be observed at the absorption peak at 3464 1/cm. The peaks at 1473 and 1327 1/cm indicate the presence of $Zn(CH_3COO)_2{\cdot}2H_2O$ associated with CH_3 bending modes, as observed in previous studies [23].

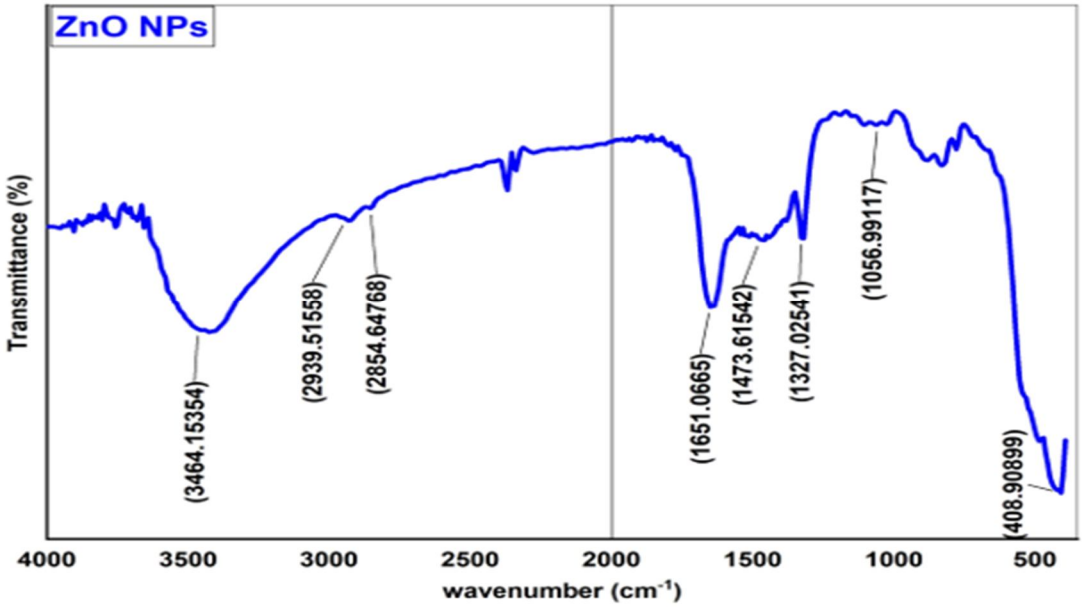

FIG. 1. FT-IR spectra of ZnO nanoparticles from 400–4000 1/cm.

An Investigation Using X-ray Diffraction

X-ray diffraction (XRD) is a non-destructive technique for studying the crystal structures of materials. Figure 2(a) displays the XRD pattern of the ZnO nanoparticles prepared by the sol-gel method, indicating the presence of the wurtzite phase. The peaks observed in the XRD pattern are consistent with the hexagonal structure of the wurtzite phase, as described in the reference code. The peaks at 2θ = 31.792°, 34.452°, 36.272°, 47.555°, 56.664°, 62.875°, 66.434°, 67.992°, 69.113°, 72.526°, and 77.093° are several sharp diffraction peaks. These peaks correspond to (1 0 0), (0 0 2), (1 0 1), (1 0 2), (1 1 0), (1 0 3), (2 0 0), (1 1 2), (2 0 1), (0 0 4), and (2 0 2) according to card number 01-079-0206 [25, 26]. Scherer's formula [27] was used to determine the crystallite size:

$$D = 0.89\lambda / (\beta\cos\theta) , \quad (1)$$

where λ is the wavelength of the X-ray (0.1541 nm), βi is the FWHM (full width at half maximum) in radians, θ is the diffraction angle, and D is the particle diameter.

Based on this calculation, the average crystallite size is 15.8 nm, and the dislocation density is 0.004 nm^{-2}. The dislocation density (δ), which shows the nanoparticles' flaws, was determined using the following formula:

$$\delta = \frac{1}{D^2} \quad (2)$$

The dislocation density of ZnO nanoparticles is inversely proportional to their grain size or crystalline size. The figure clearly demonstrates that no impurities or unreacted phase peaks were present in the ZnO samples produced using the sol-gel technique. At the calcination temperature of 400 °C, the precursors were completely disintegrated, resulting in pure ZnO.

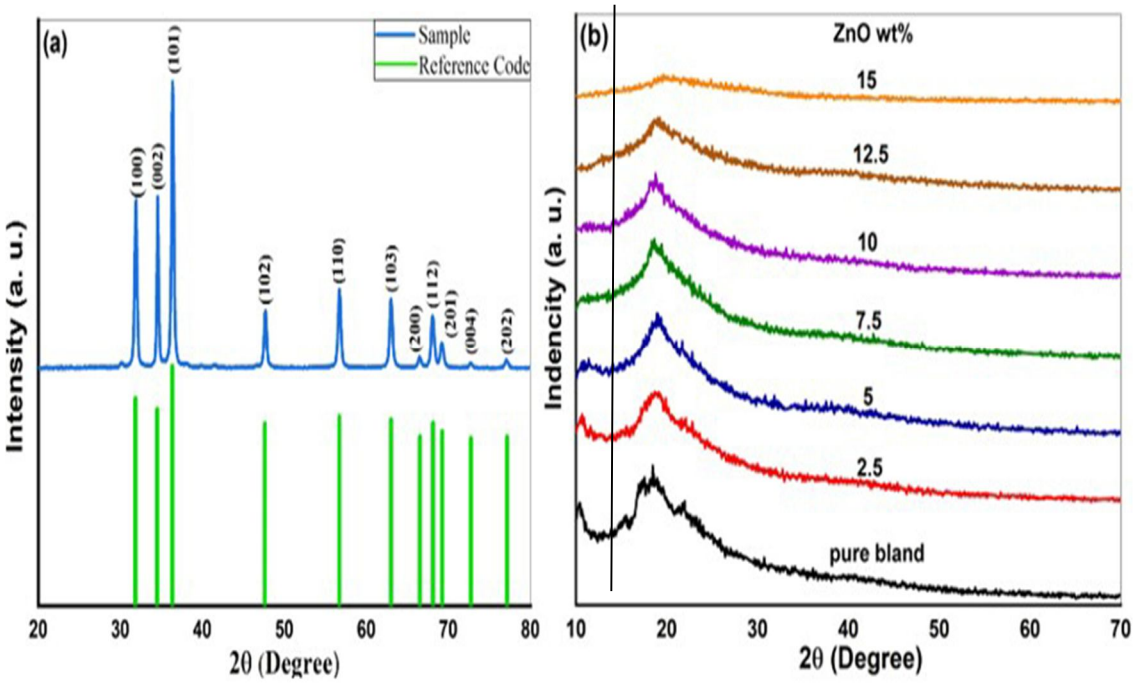

FIG. 2. XRD spectra of (a) zinc oxide nanoparticles; (b) pure Cs/PVA blend and ZnO NPs doped Cs/PVA composite.

Figure 2(b) displays the X-ray diffraction (XRD) spectrum of both the Cs/PVA polymer blend and the Cs/PVA/zinc oxide nanocomposites. The X-ray diffraction (XRD) investigation of the Cs/PVA polymer blend reveals two clearly identifiable diffraction peaks at 2θ = 10.30° and 18.23°. The prominent peak observed at 2θ = 18.58° indicates a semicrystalline structure of the pure Cs/PVA polymer blend. This is a result of the hydrogen bonding interactions that occur between the PVA and chitosan chains, both inside and between the molecules. In contrast, the XRD patterns of the Cs/PVA/zinc oxide nanocomposites display peak broadening and decreased intensity as the ZnO nanoparticle concentration increases. This indicates that the polymer blend of PVA/Cs has a larger amorphous phase when compared to pure PVA.

The decrease in intensity and concomitant increase in breadths of the XRD peaks recorded for the nanocomposite films are evidence of an increased degree of amorphization of the polymer blend owing to its interface interactions with the incorporated ZnO NPs. In the nanocomposites with higher ZnO concentrations, the broad peak present in the pure blend completely disappeared. Additionally, the absence of sharp diffraction peaks at any zinc oxide nanoparticle content suggests that the filler is effectively dispersed and fully integrated into the polymer matrix. The nanoparticles probably cause this by being embedded in the matrix's interplane gap [27, 28].

FE-SEM Analysis

Figure 3 presents FE-SEM analysis of pure ZnO's surface morphology, clearly showing ZnO nanorods with varying diameters. Zinc oxide nanostructures' antibacterial effectiveness is heavily dependent on their morphological impacts. Zinc oxide nanostructures can take many different shapes depending on the synthesis circumstances. These include rods, wires, tubes, spheres, needles, discs, rings, spirals, polyhedrons, flowers, plates, stars, and boxes. Different synthesis methods result in shapes with distinct physicochemical qualities. Moreover, rod-like nanostructures stand out as superior among their nano peers [29]. These one-dimensional nanorods, nanowires, and nanotubes offer a streamlined path for carriers, ensuring efficient transport. They reduce grain boundaries, surface imperfections, disorderliness, and short interface lengths,

providing a smooth path for both electrons and holes. Thus, besides being functional, this design is quite symbolic, but let us leave symbolic concerns for another piece and return to the analysis of nanowires. Their ability to transport electricity with minimal loss results from natural selection for conductivity optimized at the nanoscale [30]. This research has revealed that the synthesized zinc oxide possesses a rod-like morphology attributed to zinc acetate as a precursor [30]. Furthermore, the nanorod's shape is greatly influenced by the concentration of the precursor [31].

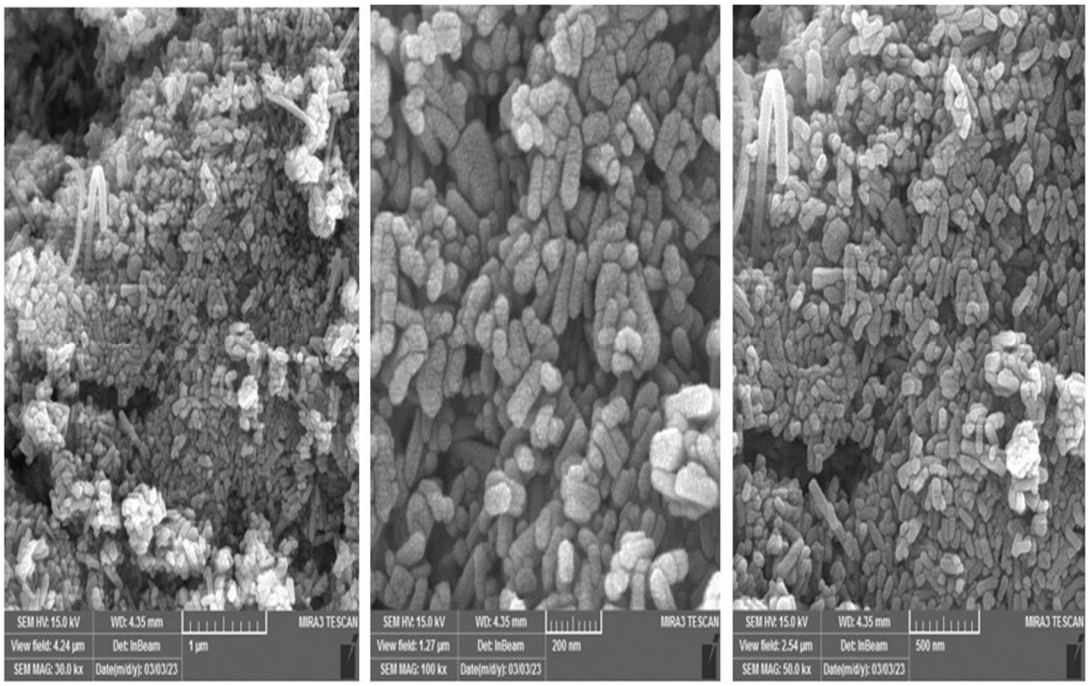

FIG. 3. FE-SEM images for zinc oxide nanoparticles.

UV-Vis Spectroscopy

UV-Vis spectroscopy, a critical technique for verifying the production of Cs/PVA/ZnO nanocomposites and determining, for example, the direct band gap energy, was used to investigate the optical absorption properties of the materials in more detail. Figures 4 and 5 show the UV-Vis spectrum of the ZnO nanostructures and the blend spectra. Figure 5(A) reveals interesting spectra: pure PVA/Cs showed a prominent absorption peak at 292 nm with a subtle shoulder at 204 nm. These features stem from its semi-crystalline structure, the PVA/Cs mixture, and the presence of C=O bonds within its structure, indicating π - π * and n - π * transitions, respectively [32–34]. Upon introduction of ZnO nanoparticles, these absorption bands significantly shifted to 212 and 240 nm. Notably, the absorption peak characteristic of zinc oxide appeared prominently at 315 nm in high-performance Cs/PVA/ZnO nanocomposites [35]. This indicates a compelling interaction between zinc oxide nanoparticles and the Cs/PVA matrix, possibly facilitated by hydrogen bonding through OH groups. Furthermore, we observed a significant redshift in the absorption edge of the material toward longer wavelengths (lower energy) with increasing concentration of zinc oxide nanoparticles within the Cs/PVA/ZnO NCs (see Fig. 5, inset B, for more clarity). This phenomenon underscores the dynamic interaction between nanomaterials and their host matrix, revealing promising approaches to customized optical and functional properties in nanocomposite materials [36].

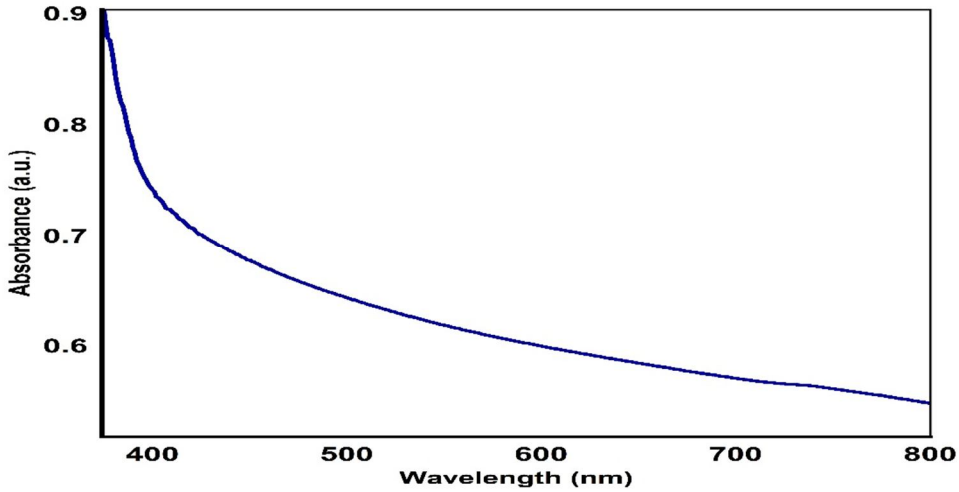

FIG. 4. UV–Vis pattern for ZnO nanoparticles.

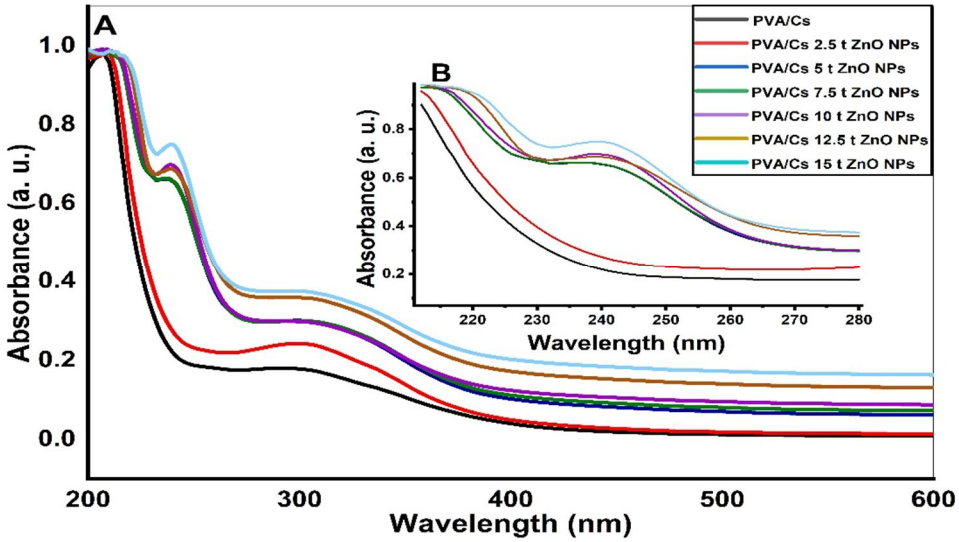

FIG. 5. UV–Vis pattern for Cs/PVA and Cs/PVA–ZnO NCs.

The optical bandgap energy (E_g) of the materials was estimated using Tauc's equation [37]:

$$(\alpha h\nu)^{1/n} = B\,(h\nu - E_g) \quad (3)$$

where hν is the energy of the incident photon and α is the absorption coefficient, which can be obtained by using the Beer–Lambert relation [38]:

$$I = I_o e^{-\propto t} \quad (4)$$

By taking the log of both sides of Eq. (4), we get:

$$\alpha(\nu) = 2.303(A/t) \quad (5)$$

where A represents the absorbance, t is the thickness of the sample, n is a numerical guide to the type of transition, B is a constant, and E_g is the optical energy gap. The value of n can be 1/2, 2, 3/2, and 3, matching up with direct and indirect, allowed or forbidden transitions. Figure 6 represents plotting $(\alpha h\nu)^2$ against hν for both the pristine blend and its ZnO NP-doped counterpart. By using Eq. (3), the energy gap is the intercept of the tangent line drawn along the sharp drop of the Tauc plot. These visuals reveal a noteworthy trend: a steady decrease in the optical energy band gap as the concentration of ZnO NPs ramps up. This shift likely arises from the intricate dance between the pure blend and the zinc oxide nanoparticles. It's not just about the mixing; those ZnO NPs seem to be crafting some intriguing defects in the Cs/PVA films. These defects set the stage for localized environments that hint at increased disorder across the samples [39]. These results are consistent with the XRD data. The values obtained for the allowed direct electron transitions are listed in Table 1.

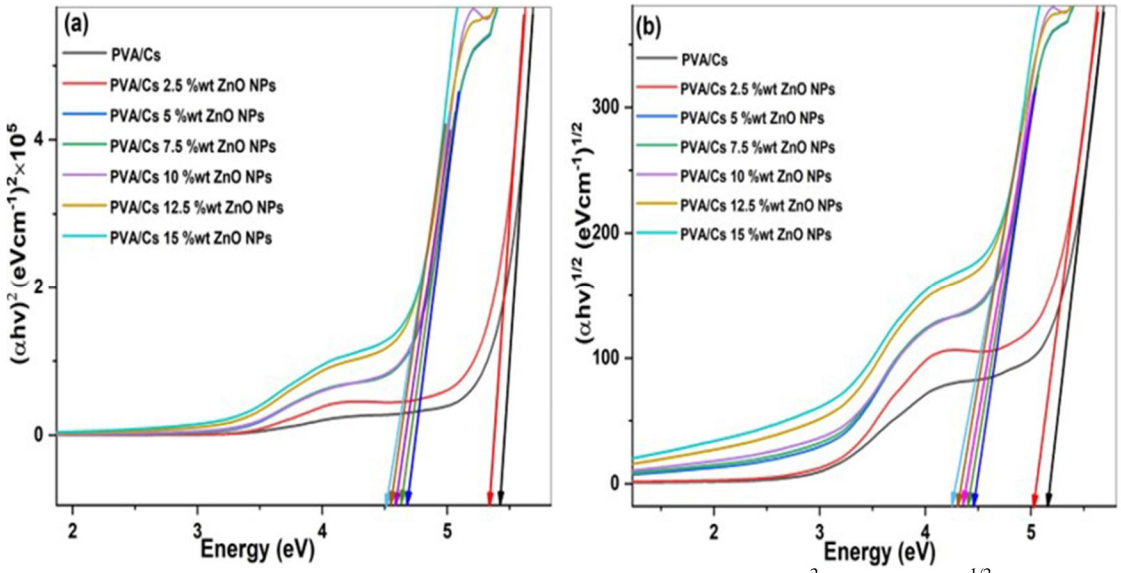

FIG. 6. Plots of for Cs/PVA and Cs/PVA–ZnO nanocomposites: (a) $(\alpha h\nu)^2$ and (b) $(\alpha h\nu)^{1/2}$ versus hν.

TABLE 1. The values of the optical energy gap (direct and indirect) for the prepared films.

ZnO/Cs-PVA (wt. %)	E_g^d(eV)	E_g^{in}(eV)
PVA/Cs	5.45	5.16
2.5	4.70	5.02
5	4.67	4.40
7.5	4.65	4.36
10	4.64	4.32
12.5	4.61	4.26
15	4.50	4.25

Antibacterial Activity Study

The widely employed agar well diffusion strategy serves as a standard method for evaluating the antimicrobial activity. Nanoparticles stand out as a compelling option for antibiotics due to their ability to exert a wide-ranging antibacterial impact, even at minimal doses. Their effectiveness spans across diverse bacterial strains, making them a promising solution in the fight against infections [40]. The mixture of PVA-Cs polymer and nanocomposites with different ratios (2.5, 5, 7.5, 10, 12.5, and 15 wt% ZnO NPs) was used to study the antibacterial activity against *Brevibacterium epidermidis*, an obligate aerobe, mesophilic, and Gram-positive bacterium isolated from human skin [17]. As shown in Figs. 7 and 9, the agar disk diffusion method was used to measure antibacterial sensitivity by determining the diameter of inhibition zones in millimeters (Table 2). The findings revealed that while the polymer alone exhibited minimal antimicrobial effect against *Brevibacterium epidermidis*, the nanocomposite samples displayed notable antibacterial activity. Incorporation of zinc oxide nanoparticles distinctly boosted this activity, showing a clear upward trend with increasing nanoparticle concentration, peaking at 15 wt. % ZnO NPs. As the amount of zinc oxide in the nanocomposites rose, so did the diameter of inhibition zones, culminating in maximum effectiveness at the highest nanoparticle concentration tested. These results vividly demonstrate how the presence of ZnO nanoparticles enhances antimicrobial performance, underscoring their potential in combating bacterial threats.

Zinc oxide nanoparticles exert their broad-spectrum antibacterial activity through several mechanisms, including ROS such as OH^-, H_2O_2, and O^{2-}, as well as disruption of the bacterial membrane [41]. The ROS damage bacterial cellular components—proteins, DNA, and lipids—due to their high reactivity and redox potential [42]. As illustrated in Fig. 8, ZnO nanoparticles interact with bacterial cells: negatively charged hydroxyl radicals and peroxides act on the bacterial surface, while H_2O_2 molecules penetrate the cell wall, causing bacterial cell damage, structural disruption, and ultimately, cell death [43]. Then, it can be

suggested that ZnO nanoparticles covalently attached to bacteria may not have any antibacterial effect, even if the bacteria are killed or survive. However, inactivation caused by their presence in growth media continues to release peroxides, enhancing bactericidal efficacy over time. Moreover, zinc ions (Zn^{2+}) released from ZnO nanoparticles enhance the antimicrobial ability of these nanoparticles due to the effect of these ions on microorganism cell membranes and intracellular components, including mitochondrial membranes and physiological processes such as active transport and acid metabolism. This ultimately leads to swelling of the bacterial cells, which in turn leads to rupture of the cell membrane and thus rupture of the bacterial cells and leakage of DNA, proteins, and lipids. Therefore, the combined effect of ROS and Zn^{2+} confirms that ZnO nanoparticles are indeed an effective mechanism for bacterial inactivation [44].

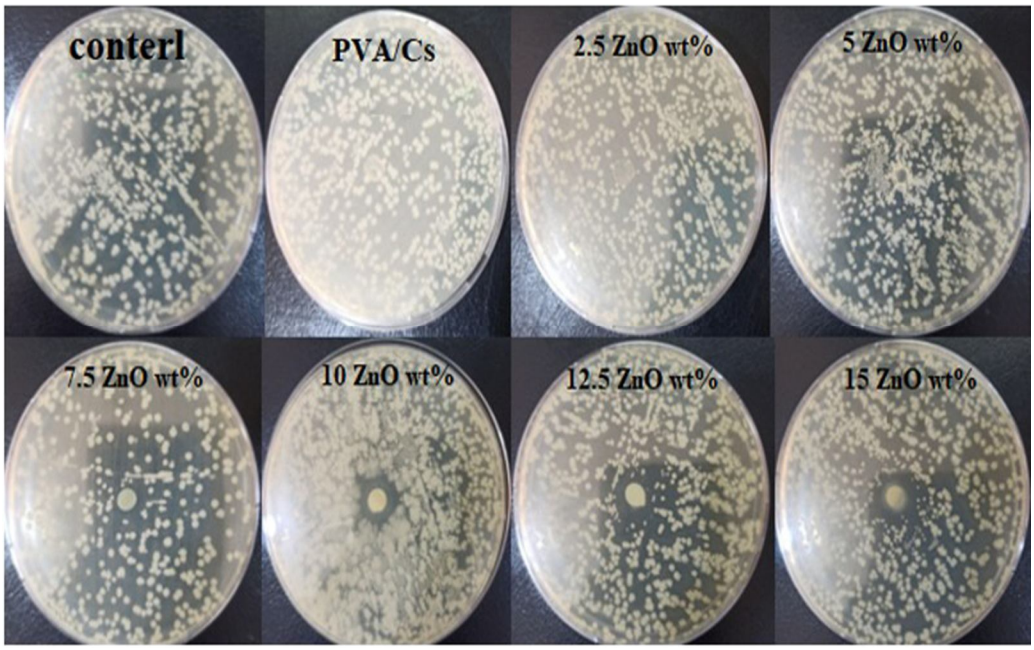

FIG. 7. Images for inhibition zones of Cs/PVA and Cs/PVA/ZnO NPs against *Brevibacterium epidermidis* bacteria.

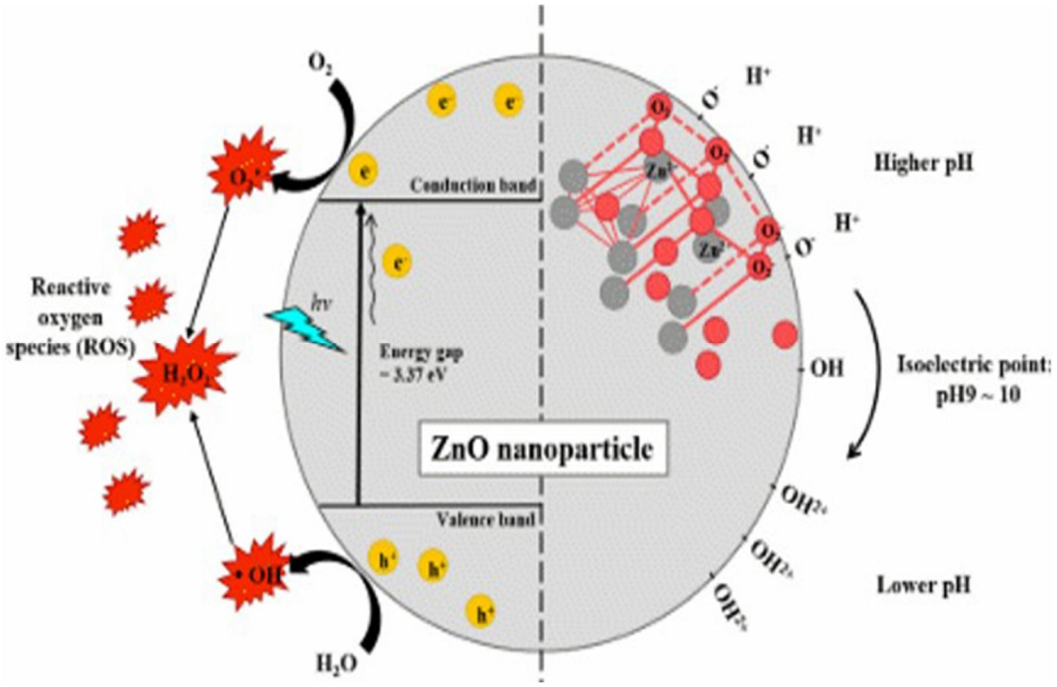

FIG. 8. Qualities of ZnO NPs influenced by their structure [45].

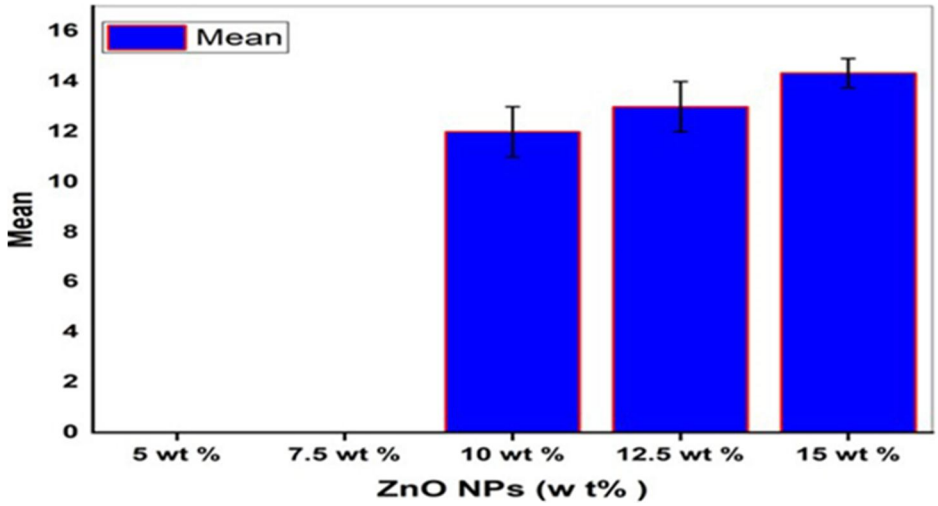

FIG. 9. The antibacterial activity of Cs/PVA and Cs/PVA/ZnO NPs against *Brevibacterium epidermidis* bacteria.

TABLE 2. Inhibition zones and mean of NCs against bacterial strains.

Sample	Inhibition zones (mm)			Mean ± S. D.
PVA-Cs	0	0	0	0
PVA/Cs 2.5 wt.% ZnO NPs	0	0	0	0
PVA/Cs 5 wt.% ZnO NPs	0	0	0	0 a
PVA/Cs 7.5 wt.% ZnO NPs	0	0	0	0 a
PVA/Cs 10 wt % ZnO NPs	13	11	12	12.000±1.000 b
PVA/Cs 12.5 wt. % ZnO NPs	14	12	13	13.000±1.000 b
PVA/Cs 15 wt. % ZnO NPs	15	14	14	14.333±0.5773 c
There is no significant difference ($p>0.05$) because the vital coefficients have similar letters.				

Conclusions

In this research, zinc oxide nanoparticles prepared by the sol–gel method were incorporated into chitosan (Cs) and polyvinyl alcohol (PVA) blend films to fabricate nanocomposites by the casting method. As evident from the infrared spectrum obtained from the Cs/PVA blend with incorporated ZnO NPs, characteristic absorption bands in the range of 2000–1250 cm^{-1} are found to change. These changes indicate the interaction of zinc ions with the polymer matrix, which can be in the form of coordination or hydrogen bonding. Such reactions are important because they can change the physical and/or chemical properties of the compound, improving the suitability of the product for various uses. XRD analysis further revealed structural modifications of the Cs/PVA matrix with increasing ZnO content, indicated by reduced peak intensities and shifts in diffraction angles, evidencing strong nanoparticle–polymer interactions. These structural changes indicate the presence of ZnO nanoparticles in the polymer network and may also lead to new composite properties. Furthermore, UV and visible analyses revealed a reduction in the optical band energy (both direct and indirect) of the Cs/PVA blend when ZnO nanoparticles were added. This decrease indicates significant changes in the electronic state of the material. The enhancement of the interfacial contacts between ZnO nanoparticles (NPs) and the polymer matrix can be credited for this improvement. These interactions can create new electronic states and hybridization effects, further enhancing optoelectronic performance. The dispersion of ZnO nanoparticles also increased the antimicrobial activity of the nanocomposite samples. Therefore, this can be attributed to the bactericidal properties of zinc oxide, which act through mechanisms such as ROS formation, Zn^{2+} ion release, and microbial

cell wall destruction. Moreover, due to the high surface area of ZnO nanoparticles combined with the matrix (Cs/PVA), the antimicrobial activity is enhanced. All these factors lead to improved efficiency of antimicrobial property, and hence the nanocomposite is suitable for use in biomedical applications, food packaging, and coatings.

References

[1] Sabir, S., Arshad, M., and Chaudhari, S.K., World J., 2014 (2014) 1.

[2] Zhou, X.-Q., Hayat, Z., Zhang, D.-D., Li, M.-Y., Hu, S., Wu, Q., Cao, Y.-F., and Yuan, Y., Processes, 11 (2023) 1193.

[3] Moezzi, A., McDonagh, A.M., and Cortie, M.B., Chem. Eng. J., 185–186 (2012) 1.

[4] Auda, A.A., Banimuslem, H.A.J., and Kadem, B.Y., J. Nanostruct., 2023 (2023) 2251.

[5] Ismail, A.M., Menazea, A.A., Kabary, H.A., El-Sherbiny, A.E., and Samy, A., J. Mol. Struct., 1196 (2019) 332.

[6] Iber, B.T., Kasan, N.A., Torsabo, D., and Omuwa, J.W., J. Renew. Mater. 10 (2022) 1097.

[7] Lam, W.S., Lam, W.H., and Lee, P.F., Mater. (Basel), 16 (2023) 2857.

[8] Maliki, S., Sharma, G., Kumar, A., Moral-Zamorano, M., Moradi, O., Baselga, J., Stadler, F.J., and García-Peñas, A., Polym. (Basel), 14 (2022) 1475.

[9] Ruiz, G.A.M. and Corrales, H.F.Z., "Chitosan, Chitosan Derivatives and their Biomedical Applications", In: "Biol. Act. Appl. Mar. Polysaccharides", (InTech, 2017).

[10] Kouchak M., Ameri, A., Naseri, B., and Boldaji, S.K., Iran. J. Basic Med. Sci., 17 (2014) 14.

[11] Connolly, M. and De Berker, D., Am. J. Clin. Dermatol., 4 (2003) 681.

[12] Kanlayavattanakul, M. and Lourith, N., Int. J. Cosmet. Sci., 33 (2011) 298.

[13] Collins, M.D., Farrow, J.A.E., Goodfellow, M., and Minnikin, D.E., Syst. Appl. Microbiol., 4 (1983) 388.

[14] Sharquie, K.E., Noaimi, A.A., and Hameed, S.D., J. Cosmet. Dermatol. Sci. Appl., 03 (2013) 203.

[15] Haque, M.J., Bellah, M.M., Hassan, M.R., and Rahman, S., Nano Express, 1 (2020) 010007.

[16] Mahamuni, P.P., Patil, P.M., Dhanavade, M.J., Badiger, M.V., Shadija, P.G., Lokhande, A.C., and Bohara, R.A., Biophys. Rep., 17 (2019) 71.

[17] Forquin, M.-P. and Weimer, B.C., "Brevibacterium", In: "Encycl. Food Microbiol.", (Elsevier, 2014) pp. 324–330.

[18] Benson, C.E. and Tatem, L., "Successful Treatment of Brevibacterium Bacteremia Solely With Antimicrobial Therapy", (Cureus, 2021).

[19] Díez-Pascual, A.M. and Luceño-Sánchez, J.A., Polym. (Basel), 13 (2021) 2105.

[20] Revathi, T. and Thambidurai, S., Adv. Powder Technol., 29 (2018) 1445.

[21] Abdeen, Z.I., El Farargy, A.F., and Negm, N.A., J. Mol. Liq., 250 (2018) 335.

[22] Yang, K., Lin, D. and Xing, B., Langmuir, 25 (2009) 3571.

[23] Lavand, A.B. and Malghe, Y.S., J. King Saud Univ. Sci., 30 (2018) 65.

[24] Fardood, S.T., Ramazani, A., and Joo, S.W., J. Appl. Chem. Res., 11 (2017) 8.

[25] Karpuraranjith, M. and Thambidurai, S., Int. J. Biol. Macromol., 104 (2017) 1753.

[26] Malini, M., Thirumavalavan, M., Yang, W.-Y., Lee, J.-F., and Annadurai, G., Int. J. Biol. Macromol., 80 (2015) 121.

[27] Chen, R., So, M.H., Che, C.-M., and Sun, H., J. Mater. Chem., 15 (2005) 4540.

[28] Hebbar, V., Bhajantri, R.F., and Naik, J., J. Mater. Sci. Mater. Electron., 28 (2017) 5827.

[29] Yang, H., Liu, C., Yang, D., Zhang, H., and Xi, Z., J. Appl. Toxicol., 29 (2009) 69.

[30] Bahadur, H., Srivastava, A., Sharma, R., and Chandra, S., Nanoscale Res. Lett., 2 (2007) 469.

[31] Pourrahimi, A.M., Liu, D., Pallon, L.K.H., Andersson, R.L., Martínez Abad, A., Lagarón, J.-M., Hedenqvist, M.S., Ström, V., Gedde, U.W., and Olsson, R.T., RSC Adv., 4 (2014) 35568.

[32] Clémenson, S., David, L., and Espuche, E., J. Polym. Sci. Part A Polym. Chem., 45 (2007) 2657.

[33] Hemalatha, K.S., Rukmani, K., Suriyamurthy, N., and Nagabhushana, B.M., Mater. Res. Bull., 51 (2014) 438.

[34] Ambrosio, R., Carrillo, A., Mota, M., de la Torre, K., Torrealba, R., Moreno, M., Vazquez, H., Flores, J., and Vivaldo, I., Polym. (Basel), 10 (2018) 1370.

[35] Urbach, F., Phys. Rev., 92 (1953) 1324.

[36] Abdelfattah, E.M., Elzanaty, H., Elsharkawy, W.B., Azzam, M.A., Elqahtani, Z.M., Alotibi, S., Alyami, M., and Fahmy, T., Polym. (Basel), 15 (2023).

[37] Morsi, M.A., El-Khodary, S.A., and Rajeh, A., Phys. B Condens. Matter., 539 (2018) 88.

[38] Abdelrazek, E.M., Elashmawi, I.S., El-khodary, A., and Yassin, A., Curr. Appl. Phys., 10 (2010) 607.

[39] Kandulna R. and Choudhary, R.B., Polym. Bull., 75 (2018) 3089.

[40] Herman, A. and Herman, A.P., J. Nanosci. Nanotechnol., 14 (2014) 946.

[41] Perelshtein, I., Ruderman, E., Perkas, N., Tzanov, T., Beddow, J., Joyce, E., Mason, T.J., Blanes, M., Mollá, K., Patlolla, A., Frenkel, A.I., and Gedanken, A., J. Mater. Chem. B, 1 (2013) 1968.

[42] Xie, Y., He, Y., Irwin, P.L., Jin, T., and Shi, X., Appl. Environ. Microbiol., 77 (2011) 2325.

[43] Zhang, L., Jiang, Y., Ding, Y., Povey, M., and York, D., J. Nanopart. Res., 9 (2007) 479.

[44] Sirelkhatim, A., Mahmud, S., Seeni, A., Kaus, N.H.M., Ann, L.C., Bakhori, S.K.M., Hasan, H., and Mohamad, D., Nano-Micro Lett., 7 (2015) 219.

[45] Sharma, P., Jang, N.Y., Lee, J.W., Park, B.C., Kim, Y.K., and Cho, N.H., Pharmaceutics, 11 (2019) 6.